



Thickness and microstructure effect on hydrogen diffusion in creep-resistant 9% Cr P92 steel and P91 weld metal

Michael Rhode^{1,2} · Tim Richter¹ · Tobias Mente¹ · Peter Mayr³ · Alexander Nitsche⁴

Received: 12 August 2021 / Accepted: 16 November 2021
© The Author(s) 2021

Abstract

Martensitic 9% Cr steels like P91 and P92 show susceptibility to delayed hydrogen assisted cracking depending on their microstructure. In that connection, effective hydrogen diffusion coefficients are used to assess the possible time-delay. Limited data on room temperature diffusion coefficients reported in literature vary widely by several orders of magnitude (mostly attributed to variation in microstructure). Especially P91 weld metal diffusion coefficients are rare so far. For that reason, electrochemical permeation experiments had been conducted using P92 base metal and P91 weld metal (in as-welded and heat-treated condition) with different thicknesses. From the results obtained, diffusion coefficients were calculated using to different methods, time-lag, and inflection point. Results show that, despite microstructural effects, the sample thickness must be considered as it influences the calculated diffusion coefficients. Finally, the comparison of calculated and measured hydrogen concentrations (determined by carrier gas hot extraction) enables the identification of realistic diffusion coefficients.

Keywords Creep resisting materials · Diffusion · Hydrogen embrittlement · Weld metal

1 Introduction

Martensitic 9% Cr steels like P91 (X10CrMoVNb9-1) or P92 (X10CrWMoVNb9-2) are widely used for fossil or nuclear power plants due to their excellent creep and corrosion resistance [1, 2]. Due to worldwide efforts to eliminate CO₂ emissions completely, these materials are also becoming increasingly important as structural materials for latent

heat storage systems [3] or as candidate materials for future fusion reactor applications [4].

1.1 Welding of 9% Cr steels

Typically, fusion welding is carried out for component fabrication. The ferritic-martensitic microstructure demands careful welding fabrication [2]. The welding process of martensitic Cr steels itself is followed by a multi-step heat treatment procedure:

- (1) After welding, the components are cooled down to a temperature around 80 °C to limit thermally induced stresses and to ensure a fully martensitic transformation. Subsequently, a hydrogen removal heat treatment (HRHT) or dehydrogenation heat treatment (DHT) is carried out, followed by cooling the joint to room temperature. It is essential for avoidance of hydrogen assisted cracking (HAC).
- (2) Finally, the welded component is subjected to the post weld heat treatment (PWHT). It is performed at temperatures ≥ 700 °C [2, 5, 6] to reduce the welding residual stresses and to induce the desired metallurgical effects like partial dissolution of carbides and tempering of

Recommended for publication by Commission IX - Behaviour of Metals Subjected to Welding

✉ Michael Rhode
michael.rhode@bam.de

¹ Department 9 - Component Safety, Bundesanstalt für Materialforschung und -prüfung (BAM), Unter den Eichen 87, 12205 Berlin, Germany

² Institute for Materials Science and Joining Technology, Otto-von-Guericke-University Magdeburg, Universitätsplatz 2, 39106 Magdeburg, Germany

³ Department of Mechanical Engineering, Chair of Materials Engineering of Additive Manufacturing, Technical University of Munich, Boltzmannstr. 15, 85748 Garching, Germany

⁴ Institute for Joining and Assembly, Chair of Welding Engineering, Technische Universität Chemnitz, Reichenhainer Strasse 70, 09126 Chemnitz, Germany

martensite that typically improve the mechanical properties (toughness, i.e., higher fracture resistance.)

If HRHT/DHT is not applied (or done wrong in terms of insufficient holding time), HAC is a considerable risk [7–10], especially for thick section weld joints. HAC is a result of the interdependencies of three critical factors: certain hydrogen concentration coupled with a mechanical load within susceptible microstructure [11, 12] like the limited ductility of hardened martensite in P91/P92 weld joints (degradation of ductility and toughness) [8, 10, 13–15]. Hydrogen sources are numerous as are the countermeasures for avoidance of HAC in the welded joints. Those include in accordance with [16, 17], the “bake-out” of consumables before welding and a clean workpiece surface (no H-containing contaminants like grease or condensates in case of on-site welding in humid atmosphere).

1.2 Hydrogen diffusion in 9% Cr steels

Hydrogen diffusion generally follows a temperature dependency, see Eq. (1).

Temperature dependence of diffusion

$$D = D_0 * e^{-\frac{E_A}{R * T}} \quad (1)$$

where “ D_0 ” is a material-specific constant, “ D ” is the temperature dependent diffusion coefficient, and the exponential factor is the Boltzmann factor with “ E_A ” as activation energy for diffusion (in kJ/mol), “ R ” is the universal gas constant (8.3145 J/mol*K), and “ T ” is the absolute temperature in K. Diverse diffusion coefficients are available in literature for low alloyed Cr–Mo(-V) steels [10, 13, 18–21]. They are used, e.g., for DHT-recommendations (temperature and holding times [22–26]). Diffusion coefficients for 9% Cr steels are limited [10, 26–29] in particular for the weld metal (WM). Table 1 shows selected minimum and maximum diffusion coefficients of low- and high-alloyed Cr–Mo steels.

Generally, the diffusion coefficients of low-alloyed Cr–Mo steels (like T/P22 or T/P24) are higher than those of the high-alloyed 9% Cr (like P91). This behavior is influenced by the chemical composition, the heat-treatment condition, and the micro-structure [10, 27, 28]. Literature suggests contrary diffusion coefficients for a respective temperature level. In accordance with Eq. (1), this behavior is confusing and demonstrates the necessity of reliable diffusion coefficients. In [28], a deviation of one magnitude has already been reported for the same 9Cr-1Mo-steel in different heat treatment conditions. But this deviation is also influenced by experimental boundary conditions like the sample thickness [30, 31].

The focus of this study is the microstructure and heat treatment effect on hydrogen diffusion in P92 and P91 multi-layer weld metal under consideration of the sample thickness. For that purpose, electrochemical permeation experiments were carried out, and the corresponding hydrogen diffusion coefficients and absorbed hydrogen concentration were calculated.

2 Materials and methods

2.1 Investigated materials and sample machining

Two different commercially available creep-resistant 9% Cr steels were investigated: (1) the base material (BM) section of a P92/X10CrWMoVNb9-2 steel tube (from VMT — former Vallourec and Mannesmann Tubes) with an inner diameter of 88.9 mm, a wall thickness of 17.5 mm, and a length of 150 mm, as seen in Fig. 1a. The BM in as-received condition was heat-treated by the following steps: normalization for 20 min at 1060 °C (air cooling) and tempering at 780 °C for 60 min (air cooling). The weld metal (WM) was made of multi-run welded P91/X10CrMoVNb9-1. For welding, a rutile-basic flux cored wire electrode (Böhler C 9 MV Ti-FD [32]) was used and deposited on a 15-mm-thick S355 low-alloyed mild steel

Table 1 Selected diffusion coefficients of high and low-alloyed creep-resistant Cr–Mo steels compared to Cr–Mo(-V) steel grades, calculated by time-lag method section 2.2)

Grade	Alloy concept in %	D_{\min} in 10^{-5} mm ² /s	D_{\max} in 10^{-5} mm ² /s	Temp. in °C	Ref
P22	2.25Cr-1Mo	1.6	3.0	25	[18]
T24	2.25Cr-1Mo-0.25 V	3.7	4.5	21	[13]
P91	9Cr-1Mo	0.1	0.4	25**	[27]
Mod. P91	9Cr-1Mo-VNbN	2.6	-	25	[29]
P91 WM	9Cr-1Mo (as-welded)	0.1	0.2	21	[26]
P91 WM	9Cr-1Mo (PWHT)	0.4	0.8	21	[26]
Mod. P91	9Cr-0.9Mo-0.21 V*	0.1	0.3	30	[28]

*Gas phase charging with 1 bar, **not given, assumed

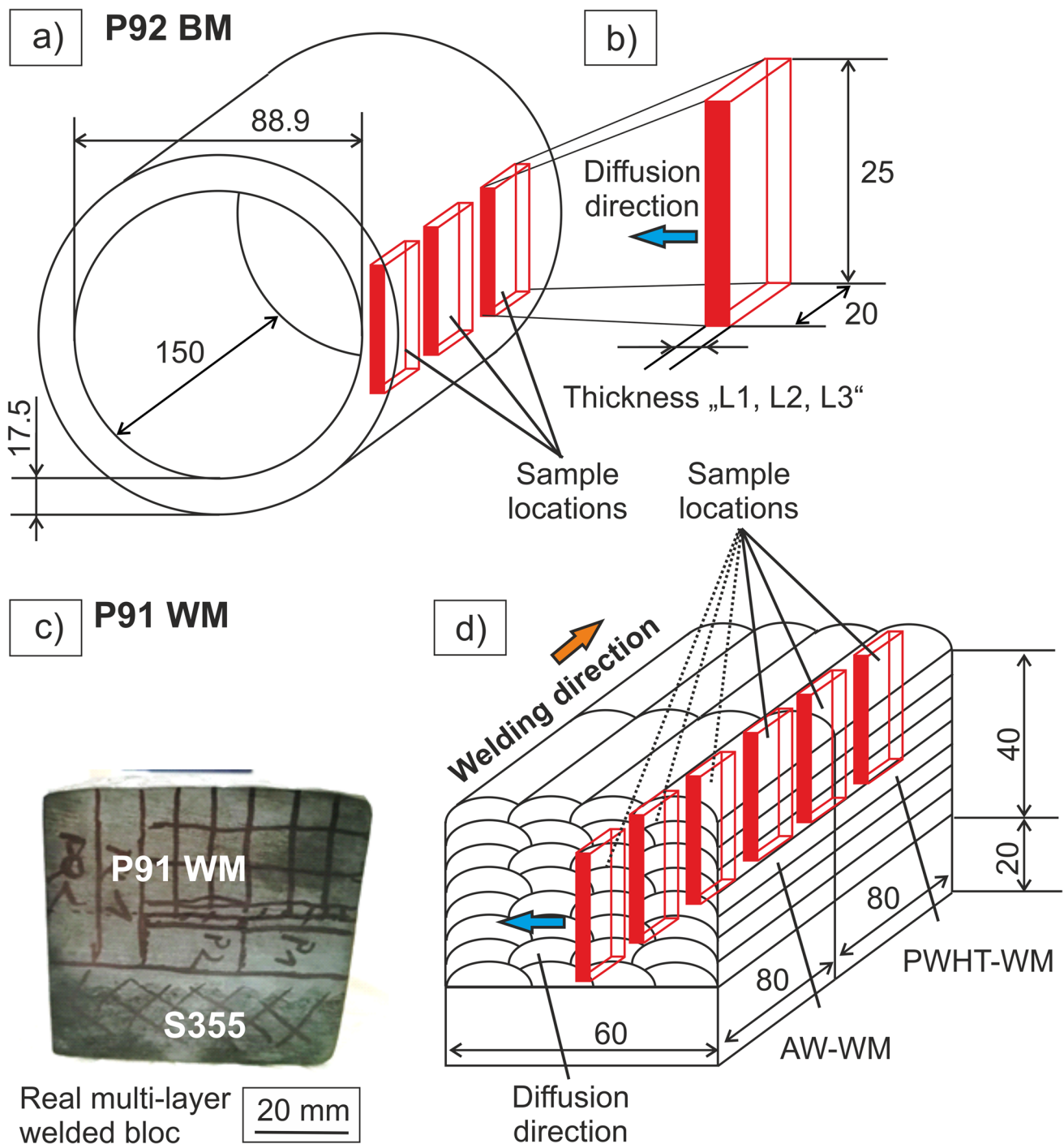


Fig. 1 P92 BM: (a) tube dimensions and (b) extracted samples; P91 WM bloc: (c) real bloc and (d) location of samples

substrate, resulting in a pure weld metal bloc with 40 mm thickness, 60 mm width, and 160 mm length, as shown in Fig. 1c. This bloc was cut into two pieces. One part was left in the as-welded (AW) condition, while the other part was further subjected to PWHT condition (further details see welding experiment).

2.1.1 Chemical composition

The chemical composition (by optical emission spectroscopy — OES) of P92 base material (BM) and P91 (WM) is listed in Table 2. The nominal chemical composition of P92 BM is fixed in [33] and P91 WM in [34].

Table 2 Composition of P92 BM [33] and P91 WM [34] (in wt.-%, Fe—balance) compared to measured composition

Grade	C
P92 BM [33]	0.13
P92 BM *	0.12
P91 WM [34]	0.13
P91 WM*	0.09
Grade	Mn
P92 BM [33]	0.60
P92 BM*	0.50
P91 WM [34]	1.20
P91 WM*	0.80
* OES determination	

2.1.2 Microstructure and hardness

The P92 BM showed a typical tempered martensitic microstructure (see Fig. 2a). Etching was carried out with Kalling's solution (micro etchant for martensitic stainless steels). The prior austenite grain boundaries are clearly visible. The micro hardness was $228 \text{ HV}0.5 \pm 5 \text{ HV}0.5$.

For the P91 WM, manual flux-cored welding (shielding gas 82% Ar and 18% CO_2) was used. The preheat temperature was 200 °C and the interpass temperature 280 °C. The WM bloc was cut into two pieces, each with a length of 80 mm. The first part remained in the AW condition; the second part was subjected to the recommended PWHT at 760 °C for 4 h [32, 34], see Fig. 1d. The aim was to get two different WM heat treatment conditions for the hydrogen diffusion experiments.

The P91 AW-WM (see Fig. 2b) is represented by a martensitic microstructure (needle-shape laths) with amounts of δ -Ferrite (identified by Lichtenegger-Blöech — LBII etchant). The hardness in AW condition was $404 \text{ HV}0.5 \pm 27 \text{ HV}0.5$. The P91 PWHT-WM microstructure (see Fig. 2c) changed to a tempered martensite, and the PWHT had a significant effect on the micro hardness ($271 \text{ HV}0.5 \pm 7 \text{ HV}0.5$). As widely accepted in literature, the microstructure is associated with precipitated MX-carbonitrides or M_{23}C_6 -carbides at the grain boundaries and martensite laths which coarsen during the PWHT [35]. For that reason, no detailed SEM/TEM-analysis was conducted.

2.1.3 Sample machining and preparation

All permeation samples were extracted by electrical discharge machining (EDM) to avoid excessive surface deformations of the samples. Therefore, the P92 BM samples were cut from the mentioned steel tube, while the P91 WM samples were extracted from the WM bloc. The thickness of the substrate plate (S355 mild steel) was 15 mm. To avoid dilution effects of substrate and P91 WM, the permeation

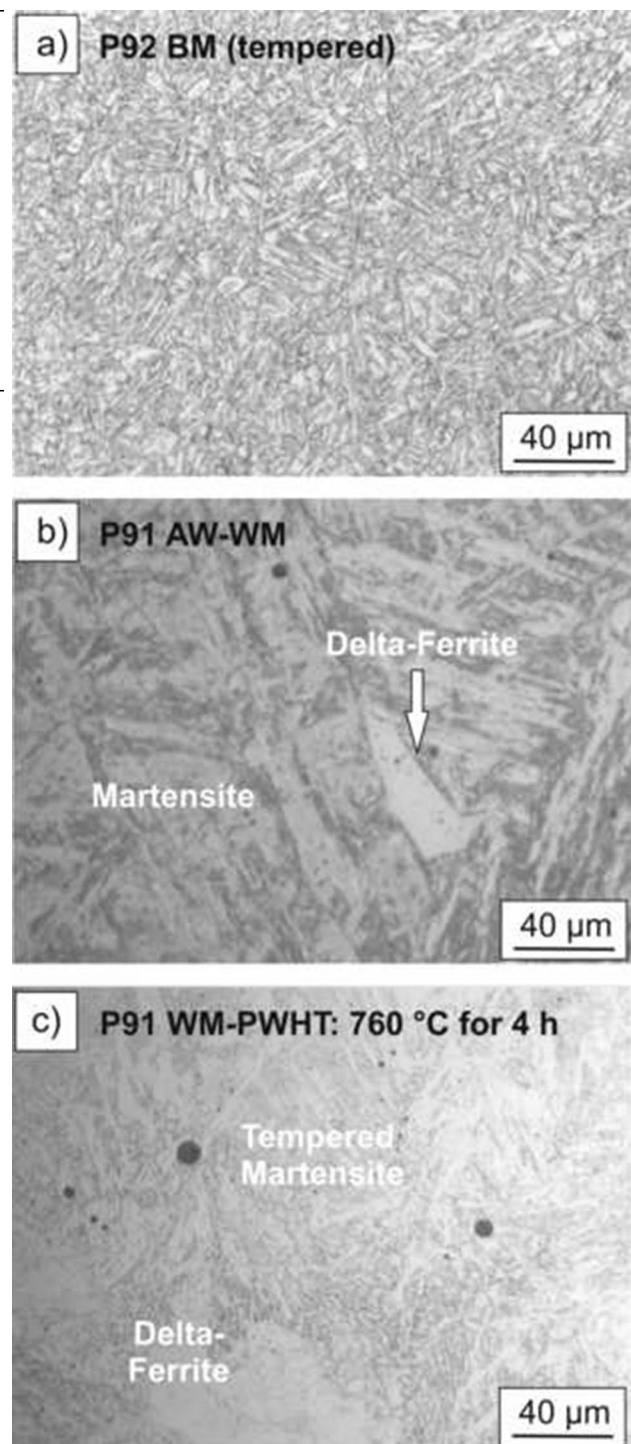


Fig. 2 Microstructure: **a** P92 BM, P91 WM in **b** AW-condition, **c** PWHT-condition (760 °C for 4 h)

samples had been extracted with a minimum distance of 5 mm to the substrate/WM interface. In addition, the sample direction was chosen in accordance with the preferred hydrogen diffusion across the multi-layer weld metal. This

case presents the typical hydrogen diffusion path from the WM into the BM via the heat-affected zone.

The locations for the sample extraction are shown in Fig. 1a (P92 BM) and Fig. 1d (P91 AW-WM and PWHT-WM). The term “L” in Fig. 1 indicates the different sample thicknesses that had been investigated. For this purpose, thin membranes with 20 mm width and 25 mm length had been machined via EDM (see Fig. 1b and d). The EDM process also offers the advantage that the machined samples are virtually free of compressive stresses that could occur by mechanical milling of the samples. In addition, the compressed region (high dislocation density) could influence the hydrogen diffusion process. Before each permeation experiment, the respective specimen was ground with SiC 500 grit paper, rinsed in ethanol for 10 min and dried in inert nitrogen gas flow for 30 s. Three different sample thicknesses had been investigated for each material grade: L1 = 0.25 mm, L2 = 0.50 mm, and L3 = 0.90 mm (BM) and 1.00 mm (WM) respectively.

2.2 Permeation experiments and diffusion coefficients

2.2.1 Permeation experiment

For the permeation experiments, an electrochemical double cell was used in accordance with [36] as fixed in ISO 17081 [37]. In general, the double-cell consists of a cathodic (–) and anodic (+) compartment, which is separated by a thin metallic membrane made from the material of interest. The experimental setup is shown in Fig. 3. All experiments were carried out at room temperature (approximately 22 °C).

The hydrogen is generated at the cathodically (–) polarized side from an acidic electrolyte (0.1 M H₂SO₄ combined with 0.05 M NaAsO₂ as recombination poison, in accordance with [13]). During the experiment, the charging electrolyte was permanently purged by Ar gas bubbling for removal of oxygen. For hydrogen charging, galvanostatic charging current of 0.60 mA/cm² was applied (by Galvanostat Wenking TG4 94, Bank Electronics). After adsorption and an absorption into the material, hydrogen diffuses through the specimen and desorbs at the anodic polarized exit side. The exit side was in potentiostatic mode with an applied potential of +200 mV vs. Ag/AgCl electrode (Wenking Potentiostat TG97, Bank Electronics and reference electrode (RE) from Xylem SI Analytics). The working electrode (WE) was a Pt 1800 type from the same company for both anodic and cathodic compartments of the permeation cell. The electrolyte was an alkaline solution of 0.1 M NaOH. The effect is that the desorbing hydrogen ions (H⁺) reduce the hydroxide ions (OH⁻) by electron transfer in accordance with Eq. (2).

Time dependent hydrogen flux



The electron transfer in Eq. (2) corresponds to the measured oxidation current (*I* in μA). Via the active hydrogen charged area (approx. 200 mm²), the oxidation current is transformed into a time-dependent permeation current density “*i*_(*t*)” in A/mm². Using the Faraday law, the hydrogen mass flux “*J*_(*t*)” can be calculated, see Eq. (3) (in accordance with [13, 36, 37]). However, “*F*” is the Faraday constant 96,485.3 As/mol and “*z*” the number of transferred electrons (= 1). The typical permeation transient shows a sigmoid-like growth (S-shape curve) for time-dependent rising hydrogen flux. After finite time, the permeation current density reaches a maximum and steady-state level of the hydrogen mass flux “*J*_{max}”. This value is used to calculate the so-called permeability “*φ*” (in mol/mm*s), see Eq. (4) and [13, 30, 31, 37]). The permeability corresponds to the maximum hydrogen flux across the specimen thickness “*L*”.

Time dependent hydrogen flux

$$J_{(t)} = \frac{i_{(t)}}{z * F} \quad (3)$$

Permeability

$$\phi = J_{\max} * L \quad (4)$$

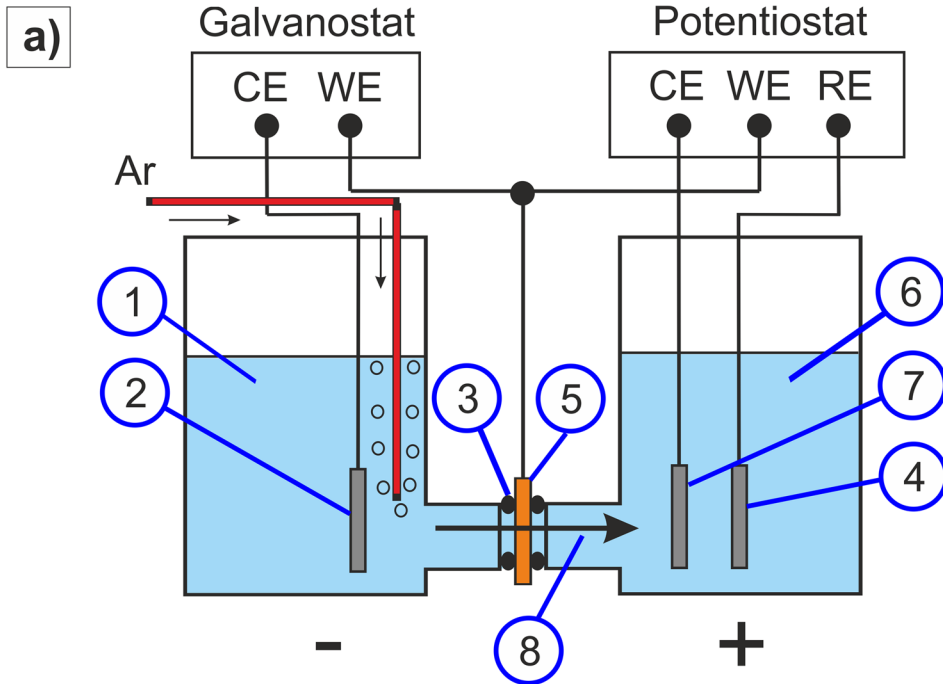
2.2.2 Calculation of diffusion coefficients

For further calculations, the permeation transient was fitted by a sigmoid growth function (Logistic5 fit, derived from the software Origin 2019). This fit function was used for continuous transient description of the permeation experiment. Based on the fitted data, the time-lag method (Fig. 3b) and the inflection point method (Fig. 3c) were used for the calculation of the hydrogen diffusion coefficients. In both schematics, “*t*_b” represents a breakthrough-time, which encompasses the time until first hydrogen is detected at the exit side. For practical implications this time, we determined this time at 1% of “*i*_{max}”. The time is referred hereafter as “*t*_{0.01}” and is calculated in accordance with Eq. (5). It represents a value of how fast hydrogen penetrates the membrane.

Definition of *t*_{0.01} time

$$t_{0.01} = f(i) = t(0.01 * i_{\max}) \quad (5)$$

The time-lag method (see Fig. 3b) uses a specific time “*t*_{lag}” after 63% of the steady-state current density is reached [37]. The diffusion coefficient “*D*_{lag}” is calculated by Eq. (6). The inflection point method (Fig. 3c) interprets the specific slope (Eq. 7) of the permeation transient at its respective inflection point (IP). This “IP” is ideally reached at 24.42% of “*i*_{max}” [38]. The corresponding diffusion coefficient “*D*_{IP}”



- ① $\text{H}_2\text{SO}_4 + \text{NaAsO}_2$
- ② CE - Counter electr. (Entrance side)
- ③ Sealings
- ④ RE - Reference electrode
- ⑤ WE - Working electr.; Specimen
- ⑥ 0.1 M NaOH (aq.)
- ⑦ CE - Counter electr. (Exit side)
- ⑧ Hydrogen flux

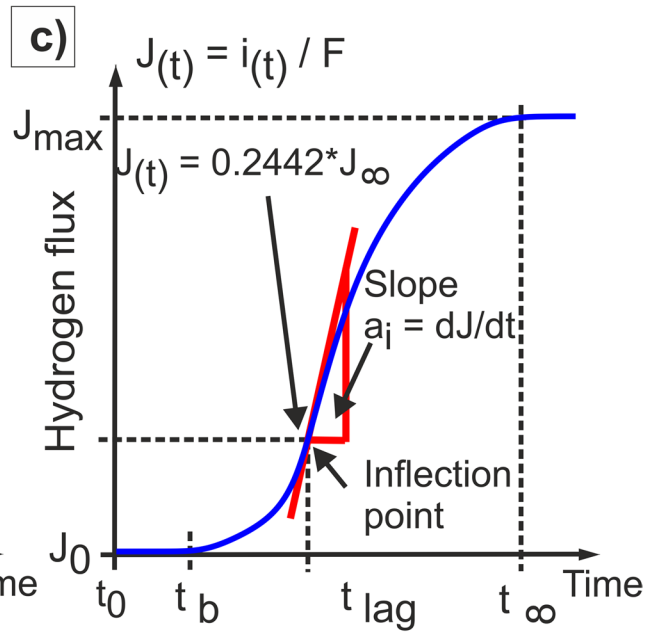
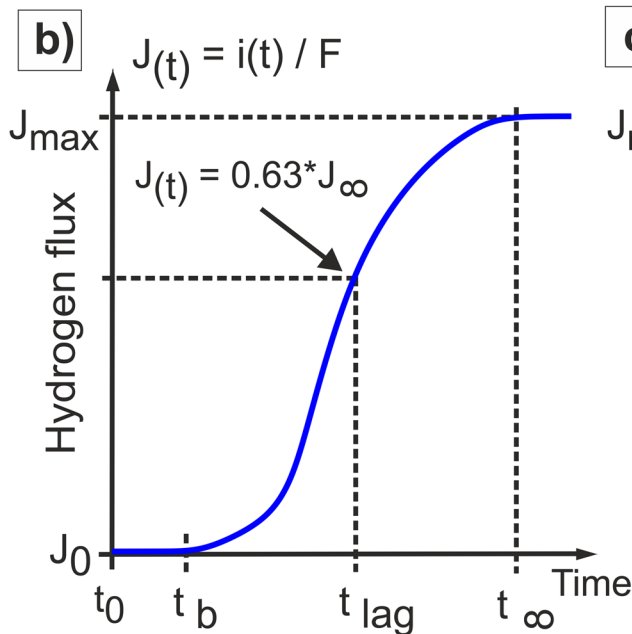


Fig. 3 Permeation: **a** experimental setup [13, 36, 37], time dependent hydrogen mass flux; determination of **b** lag-time and **c** slope at inflection point [13, 26, 36, 38]

“ is calculated by Eq. (8). For both coefficients, “ L ” is the specimen thickness of L_1 , L_2 , or L_3 .

Time-lag diffusion coefficient

$$D_{lag} = \frac{L^2}{6 * t_{lag}} \quad (6)$$

Slope at inflection point

$$a_i = \frac{di}{dt} \quad (7)$$

Inflection point diffusion coefficient

$$D_{IP} = \frac{0.04124 * L^2}{0.2442 * i_{max}} * a_i \quad (8)$$

2.3 Calculation of sub-surface hydrogen concentration and determination of real absorbed hydrogen concentration

2.3.1 Analytical calculation of sub-surface concentration

The sub-surface hydrogen concentration “ $HD_{SS,DX}$ ” is using the permeability “ ϕ ” (see Eq. 4). The subscripted “ DX ” refers to the respective diffusion coefficient “ D_{lag} ” (Eq. 6) or “ D_{IP} ” (Eq. 8). It is then calculated by Eq. (9) and given in mol/mm^3 , whereas “ DX ” refers either “ D_{lag} ” or “ D_{IP} ”.

Analytically calculated $HD_{SS,DX}$

$$HD_{SS,DX} = \frac{\phi}{DX} \quad (9)$$

The “ $HD_{SS,DX}$ ” represents the apparent hydrogen solubility of a material in terms of the corresponding absorbed hydrogen concentration from the charging electrolyte. For that purpose, a linear concentration profile in the sample is assumed in accordance with [36, 39]. Consequently, the anodic hydrogen detection cell must ensure a concentration of zero at the exit side. This presumed concentration is experimentally ensured by use of 0.1 M NaOH in the detection cell (oxidation of desorbing hydrogen atoms by OH^-) [36, 37]. Different analytically calculated “ HD_{SS} ” may result from the different diffusion coefficients (time-lag and inflection-point method).

2.3.2 Real absorbed hydrogen concentration by CGHE

For selected samples with a thickness of 0.90 and 1.00 mm, the real absorbed hydrogen concentration was measured by carrier gas hot extraction (CGHE). In this case, a sample is heated by an external heat source in a semi-open chamber, which is permanently purged with carrier gas (typically N_2). This gas mixture is transferred to a detector and analyzed. In our study, the experimentally obtained hydrogen concentration/solubility was measured using a Bruker Elementals PHOENIX G4 with a coupled thermal conductivity detector (TCD). The basic principle of CGHE technique (including calibration) is reported elsewhere [13, 40–42]. With the measured average hydrogen concentration “ \bar{C} ” (in $\text{ml}/100 \text{ g Fe}$), it is possible to calculate the apparent sub-surface hydrogen concentration “ $HD_{SS,CGHE}$ ”. The CGHE determines the hydrogen in the entire specimen ($20 \text{ mm} \times 30 \text{ mm} = 600 \text{ mm}^2 \times$ corresponding thickness, see section 2.1). But the hydrogen charged area was only 200 mm^2 . If the entire sample surface is compared to the electrochemical charged active area, a ratio of 3:1 occurs. This means that the measured hydrogen concentration must be corrected by factor 3.

Assuming a linear concentration profile in the sample, the “ $HD_{SS,CGHE}$ ” corresponds to twice the average concentration [43]. This value can be correlated to the analytically calculated sub-surface concentration “ $HD_{SS,DX}$ ” (see Eq. 9). The corresponding experimentally determined hydrogen concentration is then calculated by Eq. (10).

Measured HD_{SS}

$$HD_{SS,CGHE} = 2 * \bar{C} \quad (10)$$

In the following sections, the hydrogen concentration is given in $\text{ml}/100 \text{ g Fe}$. This value is common in welding practice and refers to the amount of diffusible hydrogen within a deposited weld metal weight of 100 g Fe (i.e., steel) [44]. The corresponding “ HD_{SS} ” (in accordance with Eq. (9) in mol/mm^3) is converted into $\text{ml}/100 \text{ g Fe}$ by Eq. (11):

Conversion of units

$$HD_{SS,DX} \left[\frac{\text{ml}}{100 \text{ g Fe}} \right] = HD_{SS,DX} \left[\frac{\text{mol}}{\text{mm}^3} \right] * V_{mH} \left[\frac{\text{ml}}{\text{mol}} \right] * V_{100 \text{ g Fe}} \left[\frac{\text{mm}^3}{100 \text{ g Fe}} \right] \quad (11)$$

In that case, “ V_{mH} ” corresponds to the molar volume of (atomic) hydrogen with 11,200 $\text{ml}/\text{mol H}$, and “ $V_{100 \text{ g Fe}}$ ” is the specific volume of 100 g Fe at room temperature (P91 and P92 steel have comparable density to pure iron) with approximately $12,800 \text{ mm}^3$ [45].

3 Results and discussion

3.1 Permeation transients

The following section presents the hydrogen permeation data for the sample thicknesses L1, L2, and L3 as well as the applied charging current densities. Figure 4 shows the obtained permeation transients for the P92 BM, while

Fig. 5 shows the values for the P91 AW and PWHT-WM (0.50 mm values from [26]). The thickness L1, L2, and L3 are abbreviated from “0.25” to “1.00”.

The obtained experimental data and the calculated values are summarized in Table 3 and encompass: the measured maximum permeation current density “ i_{\max} ”, the calculated permeability “ ϕ ”, and the time “ $t_{0.01}$ ” until the first hydrogen were detected. The diffusion coefficients were calculated by the time-lag method (“ D_{lag} ”, see Eq. 6) and the inflection

Fig. 4 P92 BM: permeation data vs. sample thickness of 0.25, 0.50, and 0.90 mm: **a** absolute data, **b** normalized data

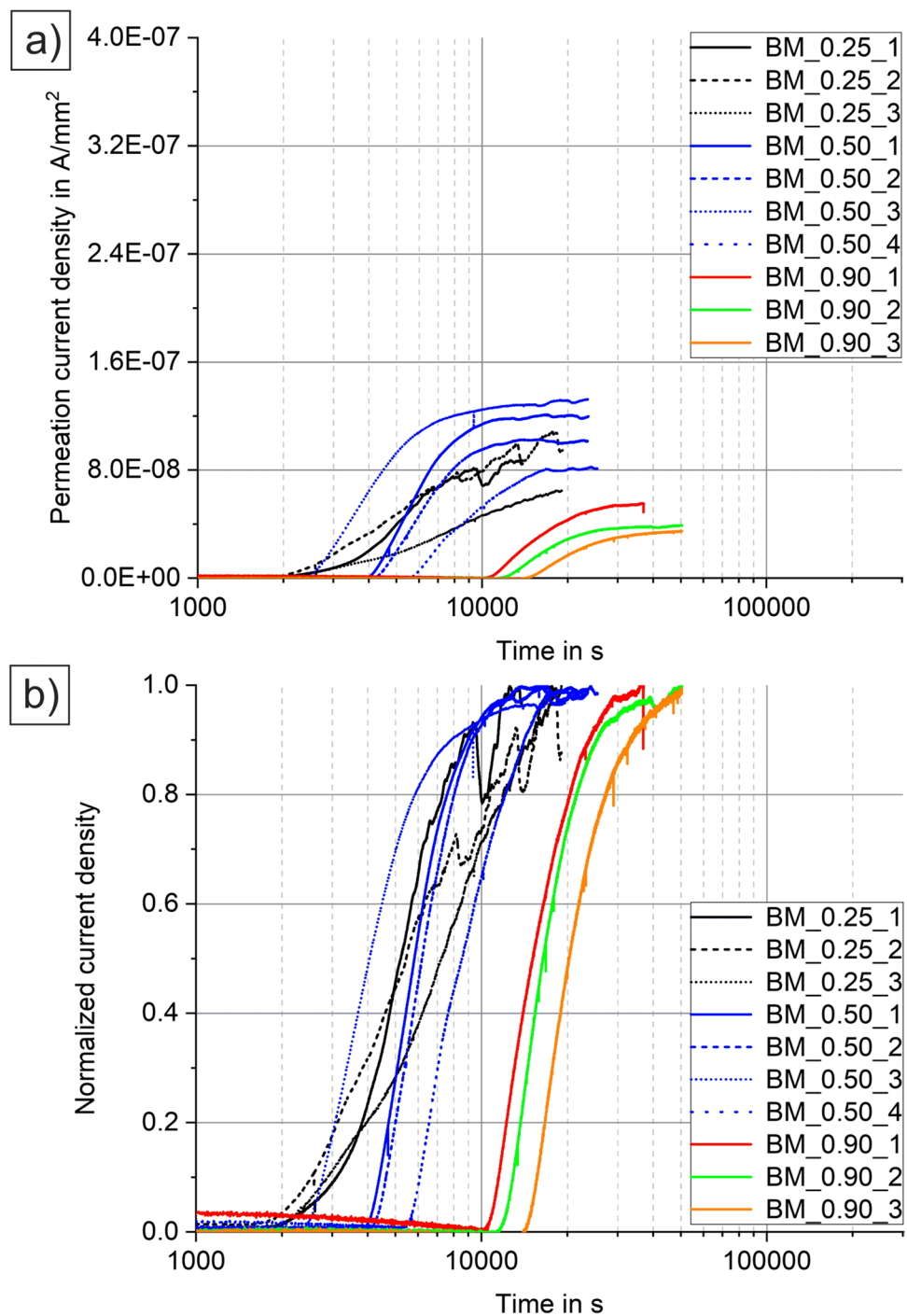


Fig. 5 P91 WM: permeation data vs. sample thickness of 0.25, 0.50 (from ref. [26]), and 1.00 mm: **a** absolute data, **b** normalized data of AW-WM and **c** absolute data, **d** normalized data of PWHT-WM

point method (“ D_{IP} ”, see Eq. 8). All investigated materials enabled stable permeation experiments. Generally, it can be ascertained that:

- The increasing specimen thickness results in delayed hydrogen diffusion, which is characterized by the necessary prolonged time to reach the steady-state condition.
- The data should be normalized to their respective maximum value and presented on logarithmic time scale. This allows the direct comparison of the slope of the experiments and an easy assessment.
- In addition, the “ i_{max} ” decreases with increasing specimen thickness. In that connection, the P91 multi-run weld metal showed approximately two times higher “ i_{max} ” compared to the P92 BM.

3.2 Discussion of material, sample thickness, and calculation method effect on hydrogen diffusion coefficients

The next sections describe how the material conditions, sample thickness, and calculation method influence the hydrogen diffusion coefficient.

3.2.1 Effect of material and heat treatment condition

Table 3 shows the summarized data of the conducted experiments for all investigated materials and their respective specimen thicknesses accompanied by the necessary data for the calculation of the diffusion coefficients. The effect of the material combines the individual contributions of the chemical composition, microstructure, and heat treatment condition. The material grade, i.e., the chemical composition, had a limited effect if the as-received (normalized and tempered) P92 BM is compared to the P91 PWHT-WM, as both materials have similar diffusion coefficients within the range of $10E-5 \text{ mm}^2/\text{s}$.

Nonetheless, the P92 has low diffusion coefficients, which is attributed to the differences in the chemical composition (see Table 2). However, if only the P91 WM is considered, the most important influence is the heat treatment condition itself as the AW condition delays the hydrogen diffusion, showing the lowest hydrogen diffusion coefficients. This is indicated by the necessary prolonged lag-time “ t_{lag} ” and the decreased permeability “ ϕ ” (see Table 3) independently of the sample thickness.

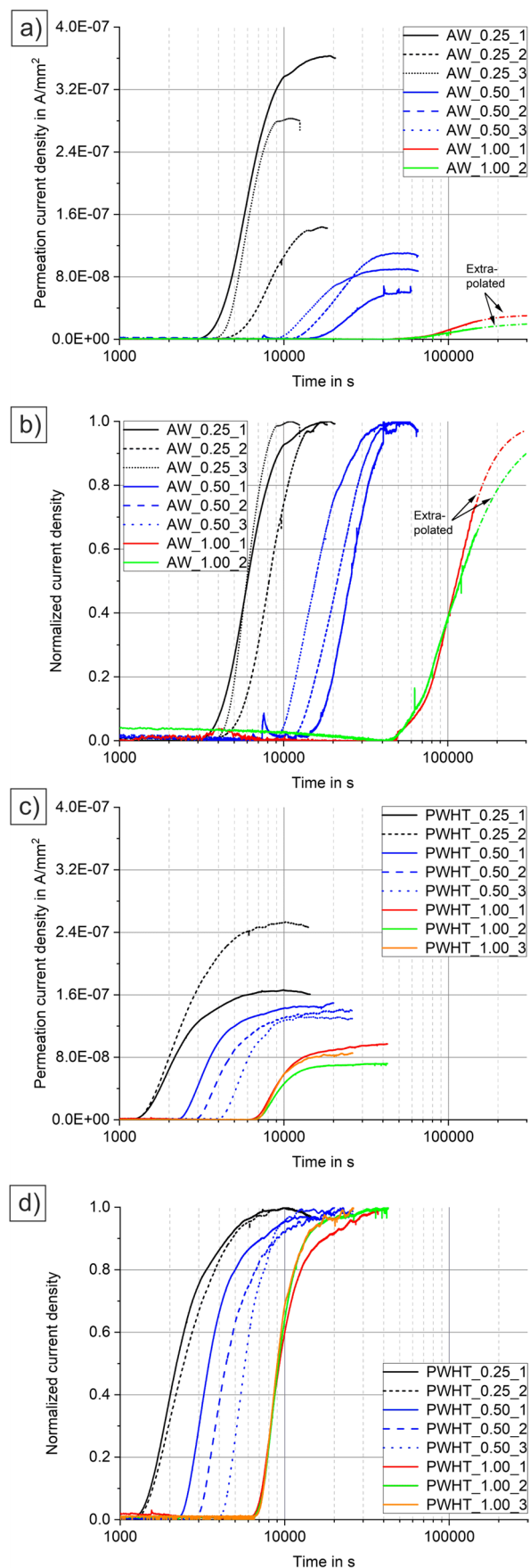


Table 3 Permeation data and calculated diffusion coefficients by time-lag and inflection point method (mean values of three experiments with standard deviation), values for 0.50 mm of P91 WM from ref. [26]

Material	<i>L</i> mm	<i>i</i> _{max} 10 ⁻⁷ A/mm ²	<i>φ</i> 10 ⁻¹³ mol/ mm*s	<i>t</i> _{0,01} s	<i>t</i> _{0,63} s	<i>a</i> _i 10 ⁻¹¹ A/mm ² *s	<i>D</i> _{lag} 10 ⁻⁶ mm ² /s	<i>D</i> _{IP} 10 ⁻⁶ mm ² /s	<i>D</i> _{lag} / <i>D</i> _{IP} -
P92 BM	0.25	0.86 ± 0.22	2.23 ± 0.57	1718 ± 264	7133 ± 1,474	1.39 ± 0.07	1.50 ± 0.29	1.67 ± 0.73	0.90
	0.50	1.09 ± 0.22	5.66 ± 1.14	3983 ± 1230	6954 ± 2227	3.14 ± 0.14	6.45 ± 1.98	11.60 ± 3.47	0.56
	0.90	0.43 ± 0.11	3.99 ± 1.05	12,044 ± 1802	19,170 ± 2941	0.44 ± 0.16	7.15 ± 1.03	13.97 ± 2.24	0.51
P91 AW-WM	0.25	2.63 ± 1.11	6.82 ± 2.87	3774 ± 411	7357 ± 1413	6.60 ± 3.64	1.45 ± 0.25	2.52 ± 0.79	0.58
	0.50	0.87 ± 0.25	4.50 ± 1.31	12,700 ± 4405	21,476 ± 3386	5.91 ± 0.21	1.98 ± 0.34	2.89 ± 0.76	0.69
	1.00	0.27 ± 0.07	2.74 ± 0.68	48,063 ± 711	136,550 ± 9829	0.024 ± 0.008	1.22 ± 0.08	1.50 ± 0.12	0.81
P91 PWHT-WM	0.25	2.10 ± 0.62	5.43 ± 1.59	1284 ± 76	2680 ± 240	11.00 ± 2.01	3.90 ± 0.35	5.64 ± 0.64	0.69
	0.50	1.57 ± 0.37	8.16 ± 1.91	4023 ± 2430	5013 ± 1175	5.03 ± 1.16	8.63 ± 2.07	13.53 ± 0.93	0.64
	1.00	0.78 ± 0.14	8.73 ± 1.43	6344 ± 86	9933 ± 306	1.87 ± 0.28	16.80 ± 0.52	35.70 ± 0.26	0.47
Average:									0.65

A prolonged hydrogen diffusion and lower permeability at the same time (independently of the sample thickness) is attributed to a higher number and efficiency of existing hydrogen traps in the P91 AW-WM compared to the tempered microstructures of the P92 BM and the P91 PWHT-WM. The significant difference of hydrogen diffusion in tempered P92 BM and the P91 WM subjected to PWHT is assumed to be a result of metallurgical effects like the reported annihilation of dislocations (and reduced density) [18] and formation and coarsening of the carbides like $M_{23}C_6$ or MX [46–48] during PWHT. These effects decrease the number of possible hydrogen traps and consequently increase the permeability and the calculated diffusion coefficients. Nonetheless, contrary opinions can be found in literature on the effect of dislocations/precipitates on hydrogen diffusion in P91 WM. On the one hand, very fine dispersed carbides are assumed as the predominant hydrogen trap in 9% Cr WM in ref. [28], but on the other hand, it is assumed in ref. [27] that dislocations also represent a predominant trap. Hydrogen trapping is very complex in high alloy steels due to its complex microstructure (grain boundaries, grain boundary area or, retained austenite, etc.). These lattice defects are necessary and influence the material properties like the creep strength, but they also represent hydrogen traps. It currently remains open, which trap is the most effective.

3.2.2 Effect of sample thickness on diffusion coefficients

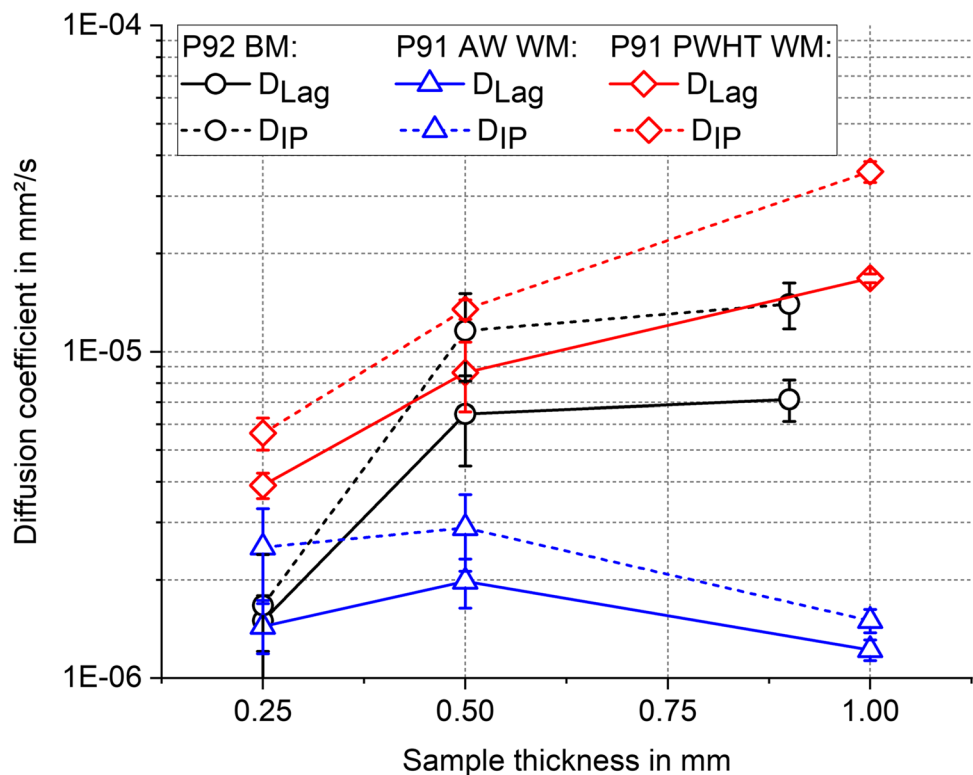
The effect of the sample thickness is obvious. With increasing sample thickness, “ i_{max} ” decreases and the necessary time to reach “ i_{max} ” significantly increases (Fig. 4a: P92 BM and Fig. 5a and c: P91 AW and PWHT-WM). If the data is normalized to the corresponding specific maximum current density ($i_{max} = 1$), the slope of the

permeation transients can be directly compared (Figs. 4b and 5b and d). The normalized curves show comparable slopes for each respective sample thickness if plotted on logarithmic time scale. This indicates that the variation of the diffusion coefficients with sample thickness should be similar. The diffusion coefficients (values shown in Table 3) are plotted vs. sample thickness in Fig. 6.

It was shown that the sample thickness has a general effect on the calculated diffusion coefficients in terms of increasing diffusion coefficients with increasing sample thickness. But this is limited to a thickness of 0.50 mm. Above this value, the coefficients significantly increase in case of the P91 PWHT-WM. The P91 AW-WM had (more or less) constant hydrogen diffusion coefficients, independently of the sample thickness. This indicates that strong hydrogen trapping occurred (see section 3.3) in the material and possible adsorption effects at the sample surface are negligible. Ideally, the sample thickness should not significantly influence the calculated diffusion coefficients. However, in case of “less-trapping” (fast hydrogen transport) materials like P92 BM and the P91 PWHT-WM, this does not appear to be true. The authors of [30, 31] confirmed this in their investigations (decreasing and delayed permeation transient with increasing specimen thickness in case of duplex stainless steel). As a result, the breakthrough time increased from minutes to hours [49].

If permeation data are used for DHT recommendations, they should be selected carefully. Nonetheless, it is obvious that the PWHT is beneficial for hydrogen diffusion. The WM in AW-condition is vice versa influenced by the delayed hydrogen diffusion (but this does not include any statement on a HAC susceptibility).

Fig. 6 Diffusion coefficients D_{lag} and D_{IP} vs. sample thickness



3.2.3 Effect of calculation method on diffusion coefficients

Both calculation methods result in different hydrogen diffusion coefficients. The ratio of " D_{lag}/D_{IP} " was between 0.47 and 0.90, which corresponds to the mean value of 0.65 (for all thicknesses presented in Table 3). Thus, the calculated diffusion coefficient " D_{Lag} " is in average 1.5 times lower than " D_{IP} ". In this regard, the time-lag method is a simple way to calculate diffusion coefficients as only the time " t_{lag} " must be determined [36, 37]. Disadvantageous is that adsorption effects from the charging electrolyte (electrochemical-sample interface, surface roughness, coverage with hydrogen atoms) are included, which are expressed in the built-up of the stable adsorption layer for hydrogen and the necessary time for hydrogen to penetrate the entire sample thickness. For practical reasons, this value is determined at 1% of the respective " i_{max} " value (denotation: " $t_{0.01}$ " time, see Table 3) in contrast to the method proposed in [37] (by extrapolation of linear part of permeation transient).

The influence of the materials investigated, and sample thickness is shown in Fig. 7. The " $t_{0.01}$ " time is plotted in log. scale vs. the sample thickness. Exponential growth functions had been used as fits. It was ascertained that the breakthrough time " $t_{0.01}$ " strongly depends on the sample thickness and increases up to one magnitude. For example, the P92 BM shows a deviation from 1718s (sample thickness of 0.25 mm) compared to 12,044 s (thickness 0.90 mm, see Table 3). If the P91 AW-WM is considered, the additional

microstructural influence is very important. In this case, the time for 0.25 mm with 3774 s increased to 48,063 s in case of 1.00 mm.

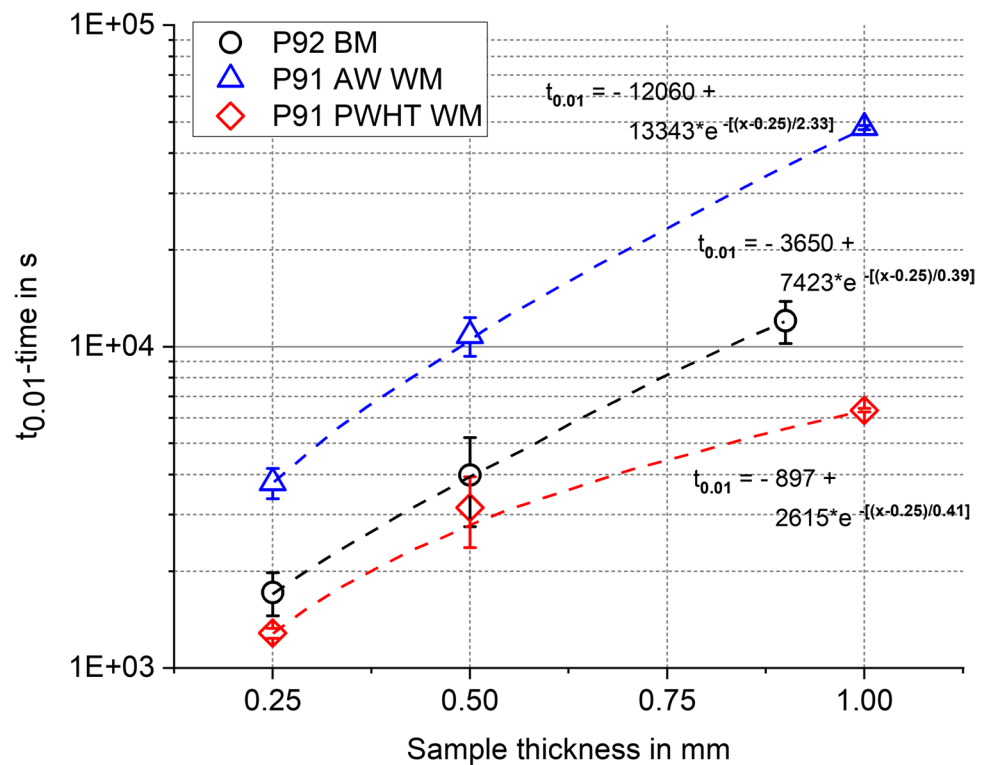
This conveys that the detected breakthrough time (until first hydrogen), strongly influences the calculated diffusion coefficient when an average time like " $t_{0.63}$ " is used, including the breakthrough time (see Eq. 6) as in the case of " D_{Lag} " and is the reason for the exponential relationship between $t_{0.01}$ and the thickness of the specimen (Fig. 7). They allow the transient definition of a microstructure dependent correlation of breakthrough time and sample thickness and show that the conventional time-lag method is practicable but perhaps not precise. The deviation of both methods was for example also reported in [13, 26, 50, 51]. In contrast, the inflection point method mostly requires a mathematical approximation by sigmoidal fit function but allows excluding absorption effects as the slope and inflection point of the regression function are used and assessed [38].

Both methods resulted in comparable hydrogen diffusion coefficients (within same magnitude of 10^{-5} mm²/s). But they have significant impact on the calculated apparent absorbed hydrogen concentration, which is presented in the next section.

3.3 Sub-surface concentrations

The " HD_{SS} " represents the apparent hydrogen solubility of a material in terms of the hydrogen concentration

Fig. 7 Breakthrough time “ $t_{0.01}$ ” dependent on material/micro-structure and sample thickness



close to the sample surface, for example absorbed from a charging electrolyte. It represents a virtual maximum concentration assuming a linear concentration profile in the sample and can be used for the assessment of hydrogen trapping efficiency.

The “ HD_{SS} ” can be calculated from the experimental data shown in Table 3 and additionally measured via CGHE (by multiplying the measured mean concentration by factor 2). This allows the comparison of the different calculation methods to the real measured values independently of the calculated diffusion coefficients.

3.3.1 Microstructure and sample thickness effects

Table 4 presents the analytically calculated sub-surface concentrations (in accordance with Eq. 9).

In Table 4, three interesting results concerning the calculated sub-surface concentration are shown: the microstructure (case 1): the P91 AW-WM had the highest concentrations, the sample thickness (case 2) has significant effect as well as (case 3) the applied calculation method.

For case 1, the already pointed out (section 3.2) higher number and efficiency of existing hydrogen traps in the P91 AW-WM is assumed to be a combination of a high number of dislocations, their density, and less-coarsened precipitates than the tempered microstructures of the P92 BM and the

Table 4 Sub-surface concentrations calculated from permeation data using D_{lag} and D_{IP} for different sample thickness

Material	Thickness L in mm	$HD_{SS,Lag}$ in 10^{-7} mol/mm ³	$HD_{SS,Lag}$ in ml/100 g Fe	$HD_{SS,IP}$ in 10^{-7} mol/mm ³	$HD_{SS,IP}$ in ml/100 g Fe
P92 BM	0.25	1.49	21.3	1.45	20.8
	0.50	0.90	12.9	0.50	7.2
	0.90	0.71	10.2	0.31	4.4
P91 AW-WM	0.25	4.83	69.3	2.72	38.9
	0.50	2.32	33.3	1.64	23.5
	1.00	2.23	31.9	1.82	26.1
P91 PWHT-WM	0.25	1.41	20.3	0.99	14.1
	0.50	0.95	13.6	0.61	8.7
	1.00	0.52	7.5	0.25	3.5

P91 PWTH-WM. The tempering decreases the number of possible hydrogen traps and consequently the calculated sub-surface concentrations.

The sample thickness itself (case 2) had a remarkable effect on the calculated sub-surface concentrations. With increasing sample thickness, the sub-surface concentration virtually decreases. In case of the P91 AW-WM (0.25 mm sample thickness), it would be 69.3 ml/100 g Fe. In case of the doubled thickness (0.50 mm), this concentration would decrease to 33.3 ml/100 g Fe. This emphasizes that the calculated sub-surface concentrations can be misleading in case of usage as value for the virtually maximum absorbed hydrogen concentration. In [52, 53], the calculated subsurface hydrogen concentration was suggested as maximum “safe” “ HD_{SS} ” value for avoidance of HAC-related defects (blisters or cracks) during permeation experiments. Hence, if the calculated sub-surface concentration is considered as maximum solubility of a given material, this value must be discussed critically. Otherwise, the calculated “ HD_{SS} ” would be misleading in terms of components vs. HAC susceptibility.

For case 3, the inflection point method resulted in higher diffusion coefficients compared to the time-lag method; the sub-surface concentration consequently increased. This demonstrates that analytical calculations are necessarily neither right nor precise. Many different variables must be considered (like absorption kinetics at the hydrogen charging side of the sample that is exposed to the charging electrolyte). A possible method to identify realistic diffusion coefficients is

to measure the real absorbed hydrogen concentration by the permeation sample during the experiment. This comparison is shown in the next section.

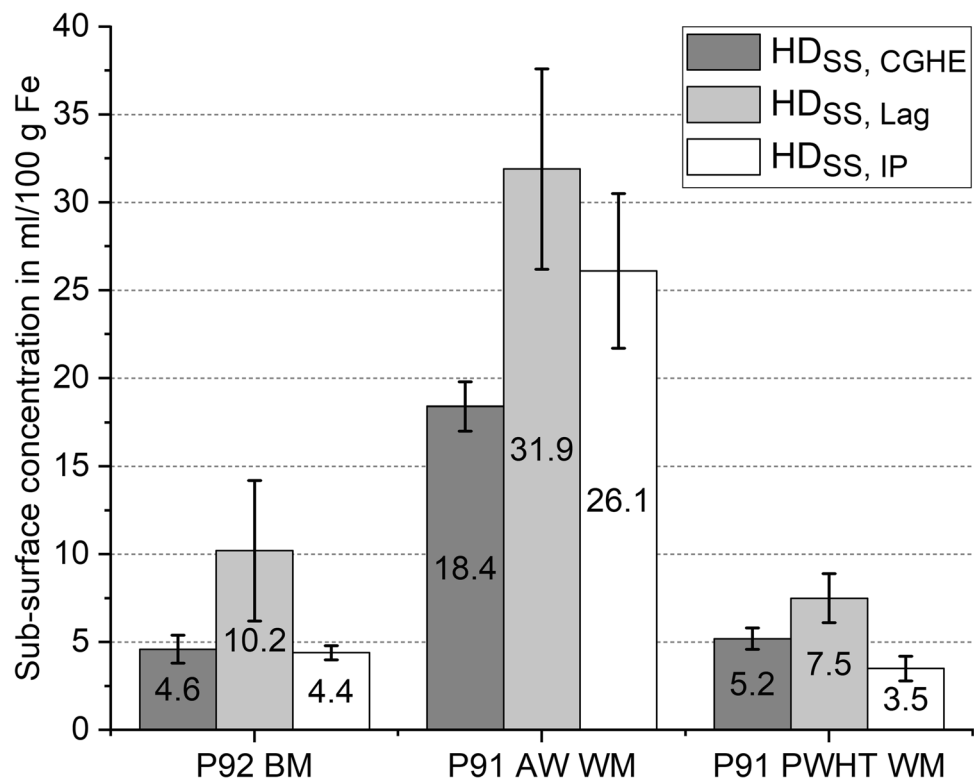
3.3.2 Comparison of calculated and measured HD_{SS}

For selected samples of P92 BM (thickness 0.9 mm) and P91 WM in both AW and PWHT condition (thickness 1.00 mm), the real absorbed hydrogen concentration during the permeation experiments was investigated. For that purpose, Fig. 8 shows the mean values of two sub-surface hydrogen concentration obtained by CGHE (Eq. 10) and compares them to the calculated values (see Table 4, in accordance with Eq. 9).

The diffusion coefficients (see Table 3) indicate significant hydrogen trapping. Consequently, the CGHE-measured sub-surface hydrogen concentration was the highest in the P91 AW-WM with 18.4 ml/100 g Fe. In contrast, the P92 BM and P91 PWHT-WM had comparable concentrations of 4.6 and 5.2 ml/100 g Fe.

If the measured sub-surface concentration “ $HD_{SS, CGHE}$ ” is compared to the analytically calculated concentrations, it is obvious that the time-lag method always resulted in the highest concentration (“ $HD_{SS, Lag}$ ” was between 7.5 and 31.9 ml/100 g Fe) compared to the inflection point method (“ $HD_{SS, IP}$ ” from 3.5 to 26.1 ml/100 g Fe). This corresponds to a deviation of approximately factor 2 and is mainly the result of the different hydrogen diffusion coefficients derived from both methods. Nevertheless, the inflection point

Fig. 8 Measured sub-surface hydrogen concentration “ $HD_{SS, CGHE}$ ” vs. calculated concentrations “ $HD_{SS, Lag}$ ” and “ $HD_{SS, IP}$ ” (for sample thickness: P92 BM = 0.90 mm, P91 WM: 1.00 mm)



method results (“ $HD_{SS, IP}$ ”) in a better accuracy to the real measured values “ $HD_{SS, CGHE}$ ”. As this general tendency was independent of the material and heat treatment condition, the inflection point method allows the calculation of more realistic sub-surface concentrations. Therefore, the “ D_{IP} ” is assumed to be suitable describing the diffusion behavior in the investigated materials. One reason is that adsorption effects are neglected in case of “ D_{IP} ” [38]. Although this method is not common, it is recommended as best-practice method for calculation of the sub-surface hydrogen concentration “ HD_{SS} ” [13, 50, 51]. This is particularly of interest when no hydrogen analyzer is available to compare the analytically calculated values to real measured values.

4 Conclusions

The focus of this study was to investigate the diffusion behavior in P92 base material and P91 multi-run weld metal in AW- and PWHT-condition. For that purpose, electrochemical permeation experiments had been carried out using three different sample thicknesses. From these experiments, the corresponding hydrogen diffusion coefficients were calculated by time-lag method [36, 37] and inflection point method [38]. Using the diffusion coefficients “ D_{Lag} ” and “ D_{IP} ” and the permeability “ ϕ ”, the apparent absorbed sub-surface concentrations “ $HD_{SS, Lag}$ ” and “ $HD_{SS, IP}$ ” had been calculated. For selected samples, these concentrations were compared to the measured concentration (by CGHE). The following conclusion can be drawn:

- This study contributes with a series of realistic hydrogen diffusion coefficients for the assessment of diffusion and HAC susceptibility. In that connection, the P92 BM was investigated in such detail for the first time. In the normalized and tempered (i.e., as-delivered) condition, the P92 BM displayed comparable diffusion characteristics to the P91 PWHT-WM. In contrast, the P91 AW-WM was characterized by delayed diffusion. In case of the AW-condition, the dislocations and their density are assumed dominant trap site.
- It still remains open if precipitates are attractive hydrogen traps in the AW-condition like the dislocations. This is because of the number and density of the precipitates (e.g., $M_{23}C_6$ and MX- precipitates) that are typically small compared to the number of dislocations. Nonetheless, due to the availability of these hydrogen diffusion coefficients, a calculation of diffusion time is now possible.
- In contrast to the diffusion theory, the effect of the thickness on the permeation transients and diffusion coefficients was visible for all three investigated material conditions. With increasing sample thickness, the maximum

permeation current density, i.e., hydrogen flux, decreases and is significantly time-delayed compared to thinner samples. This is due to the increasing length of the diffusion path and, hence, the number of hydrogen traps.

- A side-effect, which is present but not well-known, is the necessary consideration of the hydrogen adsorption reactions. This was expressed during the experiments by the so-called breakthrough time “ $t_{0,01}$ ”, which was significantly dependent on the thickness and in particular on the material. In that connection, the P91 AW-WM already required approximately 13 h (1.00 mm thickness) compared to 1 h (0.25 mm thickness) to reach 1% of the maximum current density.
- As our study demonstrated a combined effect of sample thickness and microstructure must be anticipated, which was not known in advance for the P91 and P92 steel grade family. For that reason, “exact” diffusion coefficients are hard to identify as several boundary conditions influence the calculation. In that connection, the corresponding HD_{SS} are present for the first time in this study. It was clearly ascertained that the obtained diffusion coefficients influence the “ HD_{SS} ”.
- The comparison of analytically calculated and measured HDs for P92 and P91 is presented here for the first time. In that connection, the inflection point method is closer to the measured hydrogen concentration by CGHE. Thus, the “ D_{IP} ” is recommended for use in permeation experiments instead of time-lag method coefficient “ D_{Lag} ” as recommended in [36, 37]. Based on our diffusion coefficients, a clear recommendation for industrial practice is postulated vice-versa: the time-lag method and its “ D_{Lag} ” underestimate the hydrogen diffusion. This “worst-case” scenario results in safe but long DHT dwell time for weld joints.
- The CGHE measurements for the P92 BM (0.90 mm sample thickness) and P91 WM (1.0 mm thickness) confirmed the assumption of increased trapping if hydrogen diffusion is delayed. The measured hydrogen concentration was the highest in the P91 AW-WM with approximately 18 ml/100 g Fe compared to 4 to 5 ml/100 g Fe for the P92 BM and P91 AW WM. That also means AW multi-run weld metal of 9% Cr steels has a very high capability for hydrogen trapping before PWHT is conducted. Therefore, HAC is a considerable failure mechanism for 9% Cr steels if the DHT is not carried out.

Acknowledgements Mr. Jirka Biermann is thanked for the extensive sample preparation by the EDM. Mrs. Marina Marten and Mrs. Mareike Kirstein are thanked for their assistance with the metallographic preparation. Ms. Mariam Baazaoui and Dr.-Ing. Oded Sobol are thanked for their assistance in preparing and revising this manuscript in a reader-friendly way. All aforementioned persons are with

the Bundesanstalt für Materialforschung und -prüfung (BAM), Berlin. In addition, Dr.-Ing. Lei Zhang (formerly BAM, now with Tesla Gigafactory 4, Grünheide, Germany) is thanked for her fruitful comments.

Funding Open Access funding enabled and organized by Projekt DEAL.

Availability of data The raw data is not accessible by the public but can be shared on demand with private access.

Declarations

Competing interests The authors declare no competing interests.

Open Access This article is licensed under a Creative Commons Attribution 4.0 International License, which permits use, sharing, adaptation, distribution and reproduction in any medium or format, as long as you give appropriate credit to the original author(s) and the source, provide a link to the Creative Commons licence, and indicate if changes were made. The images or other third party material in this article are included in the article's Creative Commons licence, unless indicated otherwise in a credit line to the material. If material is not included in the article's Creative Commons licence and your intended use is not permitted by statutory regulation or exceeds the permitted use, you will need to obtain permission directly from the copyright holder. To view a copy of this licence, visit <http://creativecommons.org/licenses/by/4.0/>.

References

- Hahn B, Bendick W (2008) Rohrstähle für moderne Hochleistungskraftwerke. *3R International* 47:3–12
- Coleman KK, Newell WF (2007) P91 and beyond - Welding the new-generation Cr-Mo alloys for high-temperature service. *Weld J* 86(8):29–33
- Aguero A, Audigie P, Rodriguez S, Encias-Sanchez V, de Miguel MT, Perez FJ (2017) Protective coatings for high temperature molten salt heat storage systems in solar concentration power plants. *SolarPACES2017 Conference, AIP Conference Proceedings* 2033(1):90001–1–090001–8. <https://doi.org/10.1063/1.5067095>
- Mukherjee S, Jamnapara NI (2015) Materials research and development opportunities in fusion reactors. *Proc Indian Natn Sci Acad* 81(4):827–839. <https://doi.org/10.16943/ptinsa/2015/v81i4/48299>
- Brozda J (2005) New generation creep-resistant steels, their weldability and properties of welded joints: T/P92 steel. *Weld Int* 19(1):5–13. <https://doi.org/10.1533/wint.2005.3370>
- Lojen G, Vuherer T (2020) Optimization of PWHT of simulated HAZ subzones in P91 steel with respect to hardness and impact toughness. *Metals* 10(9):1215. <https://doi.org/10.3390/met10091215>
- Husemann RU, Devrient S, Kilian R (2012) Cracking mechanism in high temperature water-T24 Root cause analysis program. In: 38th VDI-Jahrestagung Schadensanalyse in Kraftwerken. VDI-Wissensforum, Düsseldorf, p 87–103
- Hoffmeister H, Böllinghaus T (2014) Modeling of combined anodic dissolution/hydrogen-assisted stress corrosion cracking of low-alloyed power plant steels in high-temperature water environments. *Corros Sci* 70:563–578. <https://doi.org/10.5006/1048>
- Garet M, Brass AM, Haut C, Guttierrez-Solana F (1998) Hydrogen trapping on non-metallic inclusions in Cr-Mo low alloyed steels. *Corros Sci* 40:1073–1086. [https://doi.org/10.1016/S0010-938x\(98\)00008-0](https://doi.org/10.1016/S0010-938x(98)00008-0)
- Albert SK, Ramasubbu V, Parvathavarthini N, Gill TPS (2003) Influence of alloying on hydrogen-assisted cracking and diffusible hydrogen content in Cr-Mo steel welds. *Sadhana* 28:383–393. <https://doi.org/10.1007/bf02706439>
- Steppan E, Mantzke P, Steffens BR, Rhode M, Kannengiesser T (2017) Thermal desorption analysis for hydrogen trapping in microalloyed high-strength steels. *Weld World* 61:637–648. <https://doi.org/10.1007/s40194-017-0451-z>
- ISO 17462–1:2004 Destructive tests on welds in metallic materials - cold cracking tests for weldments - Arc welding processes, Part 1: General
- Rhode M (2016) Hydrogen diffusion and effect on degradation in welded microstructures of creep-resistant low-alloyed steels. BAM-Dissertationsreihe No. 148, Bundesanstalt für Materialforschung und -prüfung (BAM), Berlin, Germany
- Rhode M, Steger J, Steppan E, Kannengiesser T (2016) Effect of hydrogen on mechanical properties of a reactor pressure vessel steel grade. *Weld World* 60(4):623–638. <https://doi.org/10.1007/s40194-016-0325-9>
- Pillot S, Coudreuse L (2012) Hydrogen induced disbonding and embrittlement of steels used in petrochemical refining. In: Gangloff RP, Somerday BP (eds) Gaseous hydrogen embrittlement of materials in energy technologies, Vol. 1: The problem, its characterization and effects on particular alloy classes. Woodhead Publishing, Cambridge, pp 51–93
- Bailey N, Coe FR, Gooch TG, Hart PHM, Jenkins N, Pargeter RJ (2004) Welding steels without hydrogen cracking, 2nd revised ed. Woodhead Publishing, Oxford
- Pitrun M, Nolan D, Dunne D (2004) Diffusible hydrogen content in rutile flux-cored arc welds as a function of the welding parameters. *Weld World* 48(1–2):2–13. <https://doi.org/10.1007/BF03266408>
- Brass AM, Guillon F, Vivet S (2004) Quantification of hydrogen diffusion and trapping in 2.25Cr-1Mo and 3Cr-1Mo-V steels with the electrochemical permeation technique and melt extraction. *Metall Mater Trans A* 35:1449–1464. <https://doi.org/10.1007/s11661-004-0253-y>
- Cheng X, Cheng X, Jiang C, Zhang X, Wen Q (2018) Hydrogen diffusion and trapping in V-microalloyed mooring chain steels. *Mater Lett* 213:118–121. <https://doi.org/10.1016/j.matlet.2017.11.029>
- Valentini R, Solina A (1994) Influence of microstructure on hydrogen embrittlement behavior of 2.25Cr-1Mo steel. *Mater Sci Tech* 10(10):908–914. <https://doi.org/10.1179/mst.1994.10.10.908>
- Pereira PAS, Franco CSG, Guerra Filho JLM, dos Santos DS (2015) Hydrogen effects on the microstructure of a 2.25Cr-1Mo-0.25 V steel welded joint. *Int J Hydro Energ* 40(47):17136–17143. <https://doi.org/10.1016/j.ijhydene.2015.07.095>
- Nevasmaa P, Laukkanen A (2005) Assessment of hydrogen cracking risk in multipass weld metal of 2.25Cr-1Mo-0.25V-TiB (T24) boiler steel. *Weld World* 49(7–8):45–58. <https://doi.org/10.1007/BF03263423>
- Abe M, Nakatani N, Namatame N, Terasaki T (2012) Influence of dehydrogenation heat treatment on hydrogen distribution in multi-layer welds of Cr-Mo-V steel. *Weld World* 56:114–123. <https://doi.org/10.1007/BF03321355>
- Mente T, Böllinghaus Th, Schmitz-Niederer M (2012) Heat treatment effects on the reduction of hydrogen in multi-layer high-strength weld joints. *Weld World* 56(7/8):26–36. <https://doi.org/10.1007/BF03321362>

25. Alexandrov BT (2003) Hydrogen diffusion coefficient and modeling of hydrogen behaviour in welded joints of structural steels. *Weld World* 47(9/10):21–29. <https://doi.org/10.1007/BF03266397>
26. Rhode M, Richter T, Mayr P, Nitsche A, Mente T, Böllinghaus T (2020) Hydrogen diffusion in creep-resistant 9% Cr P91 multi-layer weld metal. *Weld World* 64(2):267–281. <https://doi.org/10.1007/s40194-019-00828-8>
27. Parvathavarthini N, Saroja S, Dayal RK (1999) Influence of microstructure on the hydrogen permeability of 9%Cr-1%Mo ferritic steel. *J Nucl Mater* 264:35–47. [https://doi.org/10.1016/S0022-3115\(98\)00486-3](https://doi.org/10.1016/S0022-3115(98)00486-3)
28. Hurtado-Noreña C, Bruzzoni P (2010) Effect of microstructure on hydrogen diffusion and trapping in a modified 9%Cr-1%Mo steel. *Mater Sci Eng A* 527(3):410–416. <https://doi.org/10.1016/j.msea.2009.08.025>
29. Padhy GK, Ramasubbu V, Murugesan N, Ramesh C, Parvathavarthini N, Albert SK (2013) Determination of apparent diffusivity of hydrogen in 9Cr-1MoVNbN steel using hot extraction-PEMHS technique. *Int J Hydrog Energy* 8:10683–10693. <https://doi.org/10.1016/j.ijhydene.2013.06.077>
30. Bouhatte J, Legrand E, Feaugas X (2011) Computational analysis of geometrical factors affecting experimental data extracted from hydrogen permeation tests: I - consequences of trapping. *Int J Hydrog Energy* 36(19):12644–12652. <https://doi.org/10.1016/j.ijhydene.2011.06.143>
31. Legrand E, Oudriss A, Frappart S, Creus J, Feaugas X, Bouhatte J (2014) Computational analysis of geometrical factors affecting experimental data extracted from hydrogen permeation tests: III – comparison with experimental results from the literature. *Int J Hydrog Energy* 39(2):1145–1155. <https://doi.org/10.1016/j.ijhydene.2013.10.099>
32. Manufacturer specification for welding wire Böhler C 9 MV Ti-FD. voestalpine Böhler Welding Group GmbH 2015
33. EN 10216-2:2014 Seamless steel tubes for pressure purposes - technical delivery conditions - Part 2: Non-alloy and alloy steel tubes with specified elevated temperature properties
34. EN ISO 17634:2015 Welding consumables - tubular cored electrodes for gas shielded metal arc welding of creep-resisting steels - Classification
35. Pandey C, Mahapatra MH, Kumar P, Saini N (2018) Some studies on P91 steel and their weldments. *J Alloys Compd* 743:332–364. <https://doi.org/10.1016/j.jallcom.2018.01.120>
36. Devanathan MAV, Stachurski Z (1963) A technique for the evaluation of hydrogen embrittlement characteristics of electroplating bath. *J Electrochem Soc* 110(8):886–890. <https://doi.org/10.1149/1.2425894>
37. ISO 17081:2014 Method of measurement of hydrogen permeation and determination of hydrogen uptake and transport in metals by an electrochemical technique
38. Dresler W, Froberg MG (1972) Über ein vereinfachtes Verfahren zur Bestimmung des Diffusionskoeffizienten von Wasserstoff in festen Metallen. *Zeitschrift für Materialkunde* 63(4):204–209
39. Crank J (1979) *The Mathematics of Diffusion*, 2nd edn. Clarendon Press, London
40. Rhode M, Schaupp T, Muenster C, Mente T et al (2019) Hydrogen determination in welded specimens by carrier gas hot extraction - a review on the main parameters and their effects on hydrogen measurement. *Weld World* 63(2):511–526. <https://doi.org/10.1007/s40194-018-0664-9>
41. Salmi S, Rhode M, Juettner S, Zinke M (2015) Hydrogen determination in 22MnB5 Steel grade by use of carrier gas hot extraction technique. *Weld World* 59:137–144. <https://doi.org/10.1007/s40194-014-0186-z>
42. Kannengiesser T, Tiersch N (2010) Comparative study between hot extraction methods and mercury method - a national round robin test. *Weld World* 54(5–6):R108–R114
43. Böllinghaus T, Hoffmeister H, Feuerstake K (1998) Finite element calculation of hydrogen uptake and diffusion in martensitic stainless-steel welds. In: Cerjak, H.; Bhadeshia, H. K. H. D. (ed.): *The Mathematical Modelling of Weld Phenomena* 4, pp 355–378
44. ISO 3690:2018 Welding and allied processes - determination of hydrogen content in arc weld metal
45. Böllinghaus T, Hoffmeister H, Feurstake K, Alzer A, Krewinkel J (1998) Finite element calculation of hydrogen uptake and diffusion in martensitic stainless-steel welds. In: Cerjak H (ed) *Mathematical Modeling of Weld Phenomena*. The Institute of Materials, London, pp 355–378
46. Fallahmohammadi E, Bolzoni F, Fumagalli G, Re G, Benassi G, Lazzari L (2014) Hydrogen diffusion into three metallurgical microstructures of a C-Mn X65 and low alloy F22 sour service steel pipelines. *Int J Hydrog Energy* 39(25):13300–13313. <https://doi.org/10.1016/j.ijhydene.2014.06.122>
47. Pandey C, Mahapatra MM (2016) Effect of heat treatment on microstructure and hot impact toughness of various zones of P91 welded pipes. *J Mater Eng Perform* 25:2195–2210. <https://doi.org/10.1007/s11665-016-2064-x>
48. El-Rahman MA, El-Salam A, El-Mahallawi I, El-Koussy MR (2013) Influence of heat input and post-weld heat treatment on boiler steel P91 (9Cr-1Mo-V-Nb) weld joints. *J Heat Treat Surf Eng* 7(1):32–37. <https://doi.org/10.1179/1749514813Z.0000000051>
49. Owczarek E, Zakroczyński T (2000) Hydrogen transport in a duplex stainless steel. *Acta Mater* 48:3059–3070. [https://doi.org/10.1016/S1359-6454\(00\)00122-1](https://doi.org/10.1016/S1359-6454(00)00122-1)
50. Seeger DM (2005) Wasserstoffaufnahme und -diffusion in Schweißnahtgefügen hochfester Stähle. No. 5, Bundesanstalt für Materialforschung und -prüfung (BAM), Berlin
51. Rhode M, Kannengiesser T, Steger J (2014) Approach for calculation of apparent hydrogen diffusion coefficients with permeation experiments in CrMoV steel weld joints. *Steel & Hydrogen 2014: 2nd International Conference on Metals and Hydrogen. Conference Proceedings*, pp 671–674
52. Kittel J, Smanio V, Fregonese M, Garnier L, Lefebvre X (2010) Hydrogen induced cracking (HIC) testing of low alloy steel in sour environment: Impact of time of exposure and on the extent of damage. *Corros Sci* 52(4):1386–1392. <https://doi.org/10.1016/j.corsci.2009.11.044>
53. Lunarska E, Ososkov Y, Jagodzinsky Y (1996) Correlation between critical hydrogen concentration and hydrogen damage of pipeline steel. *Int J Hydrog Energy* 22(2/3):279–284. [https://doi.org/10.1016/S0360-3199\(96\)00178-4](https://doi.org/10.1016/S0360-3199(96)00178-4)

Publisher's note Springer Nature remains neutral with regard to jurisdictional claims in published maps and institutional affiliations.